Reduced Order Design Optimization of Liquid Cooled Heat Sinks

Aniket Ajay Lad
Department of Mechanical Science and Engineering, University of Illinois at Urbana - Champaign
1206 West Green Street, Urbana, IL 61801, USA.
Email: aniketl2@illinois.edu

Dr. Kai A. James
Department of Aerospace Engineering, University of Illinois at Urbana - Champaign
104 South Wright Street, Urbana, IL 61801, USA.
Email: kaijames@illinois.edu

Dr. William P. King
Department of Mechanical Science and Engineering, University of Illinois at Urbana - Champaign
1206 West Green Street, Urbana, IL 61801, USA.
Email: wpk@illinois.edu

Dr. Nenad Miljkovic
Department of Mechanical Science and Engineering, University of Illinois at Urbana - Champaign
1206 West Green Street, Urbana, IL 61801, USA.
Department of Electrical and Computer Engineering, University of Illinois at Urbana–Champaign,
306 North Wright Street, Urbana, IL 61801, USA
Materials Research Laboratory, University of Illinois at Urbana–Champaign, Urbana, Illinois 61801, USA
International Institute for Carbon Neutral Energy Research (WPI-I2CNER), Kyushu University, 744 Motooka, Nishi-ku, Fukuoka, 819-0395, Japan
Email: nmiljkov@illinois.edu

Corresponding Author Emails: Nenad Miljkovic (nmiljkov@illinois.edu)
William P. King (wpk@illinois.edu)
Kai A. James (kaijames@illinois.edu)

ABSTRACT

The recent growth in electronics power density has created a significant need for effective thermal management solutions. Liquid-cooled heat sinks or cold plates are typically used to achieve high volumetric power density cooling. A natural trade-off exists between the thermal and hydraulic performance of a cold plate, creating an opportunity for design optimization. Current design optimization methods rely on computationally expensive and time consuming computational fluid dynamics (CFD) simulations. Here, we develop a rapid design optimization tool for liquid cooled heat sinks based on reduced order models for the thermal-hydraulic behavior. Flow layout is expressed as a combination of simple building blocks on a divided coarse grid. The flow layout and geometrical parameters are incorporated to optimize designs that can effectively address heterogeneous cooling requirements within electronics packages. We demonstrate that the use of population-based searches for optimal layout selection, while not ensuring a global optimum solution, can provide optimal or near-optimal results for most of test cases studied. The approach is shown to generate optimal designs within a timescale of 60-120 seconds. A case study based on cooling of a commercial silicon carbide (SiC) electronics power module is used to demonstrate the application of the developed tool and is shown to improve the performance as compared to an aggressive state-of-the-art single-phase liquid cooling solution by reducing the SiC junction-to-coolant thermal resistance by 25% for the same pressure drop.

NOMENCLATURE:

TO	Topology Optimization
OPS	Optimum Path Search
COTS	Commercial-off-the-shelf
GA	Genetic Algorithm
TIM	Thermal Interface Material
SOA	State-of-the-art
WEG50	Water and Ethylene Glycol mixture, 50% by volume
EV/HEV	Electric vehicles/ Hybrid electric vehicles
CFD	Computational Fluid Dynamics
d	Channel hydraulic diameter (m)
v	Average flow velocity (m s^{-1})
L	Fluid block size/length (m)
f	Friction factor
Re	Reynolds Number
C	Specific heat (kJ kg^{-1} K^{-1})
T	Temperature (℃)
h	Heat transfer coefficient (W m^{-2} K^{-1})
A	Area (m^2)
S	Conduction Shape Factor (m)
Pr	Prandtl Number
Nu	Nusselt Number
k	Thermal Conductivity (W m^{-1} K^{-1})

$q"$	Heat flux (W m^{-2})
P	Pressure (Pa)
$\dot{m}$	Mass flow rate (kg s^{-1})

Greek Symbols

ΔP	Pressure drop (Pa)
ρ	Density (kg m^{-3})
μ	Dynamic viscosity (N s m^{-2})
ϵ	Roughness (m)
Θ	Thermal resistance (℃ W^{-1})

Subscripts

in	Inlet
out	Outlet
f	Fluid
s	Solid
eff	Effective
c	Cross-section
l	Lateral
top	Top surface
s, max	Surface maximum
s, dev	Surface standard deviation

1. INTRODUCTION

The rapid densification of electronic systems as evident from the International Technology Roadmap for Semiconductors (ITRS) [1] has increased the demand for effective heat dissipation. Thermal management is a roadblock to further miniaturization of electronics considering safe operating condition requirements as well as performance degradation at elevated temperatures within active and passive components. Thermal and hydraulic performance along with the volume and mass of the thermal management solution at the component level as well as the auxiliary component and system level has inspired multi-disciplinary, multi-objective optimization for electro-thermal systems[2–5]. Effective cooling performance and simplicity has popularized the application of single-phase liquid cooled thermal management approaches for electronics cooling. These include channel flow heat sinks, as well as jet impingement cooling [6–8]. Seminal work on microchannel heat sinks by Tuckerman and Pease [9] demonstrated the potential of liquid cooling solutions for high heat flux removal. Enhancement in the heat transfer performance mapped in terms of the low thermal resistance of 0.1 ($^{o}C \cdot cm^2$)/W comes at the cost of high pressure drop approaching 2 bar, thus increasing demand for pumping power. Many researchers have investigated liquid cooled heat sink performance for a range of design and operating conditions using experimental [10–12], analytical [13–16] and numerical approaches [17–19]. Results of these studies have guided the design process for liquid cooled systems. Parametric modeling [20–22] of performance parameters with respect to design variables including geometric dimensions and flow boundary conditions has provided means for design optimization [23–27]. Experimental approaches have yielded the most accurate results for performance modeling but are restrictive in terms of the number of design points that can be considered due to the cost and time required in setting up the experiments for different design variations. Numerical simulations using fluid flow

and conjugate heat transfer analysis enable investigation of the necessary performance parameters. Numerical studies however need to be supported with mesh refinement and experimental validation for ensuring accuracy of the obtained results. Even though parametric studies are a proven tool for design optimization, their scope is limited in terms of design variables available for consideration. This limitation often fails to capture the complete flexibility within the design domain. Implementation of custom channel designs and flow layouts for increasing the heat transfer performance by enhancing flow mixing [28–34] is instrumental for designing high performance thermal management systems. Most past studies are constrained in a way that leads to optimization of hyper-specific designs. While providing utility at optimizing those designs, there is a need for additional research that allows for broader search of the design space and consideration of different design architectures.

Inspired by exciting developments in its application to solve problems in structural mechanics, topology optimization (TO) has been adapted for designing high performance heat sinks [35–37]. More recently, TO has been adopted for the design of liquid cooled heat sinks [38–43]. TO uses numerical simulations and sensitivity calculations for every iteration in the optimization search, which can be computationally expensive and time-consuming. Published research investigated design improvement and optimization of liquid cooled heat sinks most focuses on overall heat transfer performance at a given boundary. In practice, liquid cooled heat sinks can be subject to spatially heterogeneous temperature profiles, resulting in non-uniform heat fluxes and thermal stresses within electronics packages and reduced reliability [44,45]. Although the challenges associated with device-to-device temperature gradients have been addressed in specific studies focusing on targeted hot-spot cooling [46–48], seldom do these studies entail design optimization. Electro-thermal co-design applications use reduced order thermal

performance estimation [4]. Temporal and computational resource requirements of existing thermal design optimization approaches restrict their integration with electro-thermal co-design packages.

This paper develops a design optimization tool for single-phase liquid cooled heat sinks. The fluid flow layout is broken down into flow blocks which form elements divided into a coarser two-dimensional (2D) grid. First, the governing mass, momentum, and energy equations for fluid flow and heat transfer within fluid and solid domains [48], [49] are solved to obtain the performance of the design in terms of thermal resistance, pressure drop and temperature deviation on the heated surface. Next, an optimal fluid flow layout is found using the Optimum Path Search (OPS) algorithm based on optimization of the thermal-hydraulic performance parameters. The flow layout geometry is then further optimized by considering variable hydraulic diameters using a gradient-based optimization solver. The layout and geometry optimization are then integrated to form an overall design optimization tool. Performance modeling coupled with our rapid design method resulted in cold plate design optimization on a time scale of 60-120 s depending on design complexity. All computations were performed on an Inlet(R) Core™ i7-10700 CPU @ 2.9GHz computer using serial computing. A case study was conducted on a SiC power module, demonstrating a 25% reduction in junction-to-coolant thermal resistance for our optimized design when compared to a commercially available aggressive single-phase cold plate solution at the identical 16 kPa pressure drop.

2. PERFORMANCE MODELING

Figure 1a shows a traditional commercial-off-the-shelf (COTS) four-pass cold plate design used for a variety of electronics cooling applications. This cold plate design can be broken down into a series of simple flow blocks by dividing the geometry into a coarse grid (Figure 1b). Each grid element consists of a unique flow block. The flow blocks for a design flow can be categorized as straight blocks or elbows (Figure 1c) for non-parallel (series) flows. Fluid flow for each of the blocks modelled as internal channel flow (Figures 1d-f) is analyzed by solving flow continuity and momentum conservation equations given by:

$$d_{\text{in}}^2 v_{\text{in}} = d_{\text{out}}^2 v_{\text{out}}\,, \tag{1}$$

$$\Delta P = \frac{fL}{d}\frac{\rho v^2}{2}\,, \tag{2}$$

where $d_{\text{in}}, v_{\text{in}}$ and $d_{\text{out}}, v_{\text{out}}$ are the channel hydraulic diameter and average flow velocity at the inlet and outlet faces of the flow block, respectively, ΔP represents the pressure drop within the flow block calculated using f, ρ, L, d, and v which denote friction factor, fluid density, block size/length, average channel hydraulic diameter ($d = (d_{\text{in}} + d_{\text{out}})/2$) and average of the inlet and outlet velocities ($v = (v_{\text{in}} + v_{\text{out}})/2$), respectively.

The continuity equation ensures the conservation of mass entering and leaving each individual block. Momentum conservation provides the pressure drop in terms of the solved velocity values. Here, the Darcy friction factor is used for obtaining the pressure drop in the block in terms of inlet velocity assuming fully hydrodynamically-developed flow. The friction factor is found according to correlations given in Eqns. (3, 4) for laminar and turbulent flows. Interpolated values are used within the transition regime [49].

$$f = \frac{64}{\mathrm{Re}}; \qquad \mathrm{Re} < 2300 \text{ (Laminar)} \tag{3}$$

$$\frac{1}{\sqrt{f}} = -2\log_{10}\left(\frac{\epsilon}{3.7d} + \frac{2.51}{\mathrm{Re}\sqrt{f}}\right); \quad \mathrm{Re} > 4000 \text{ (Turbulent)} \tag{4}$$

where Re is the Reynolds number based on average diameter and fluid flow velocity (Re = $\rho v d/\mu$, where μ is the dynamic viscosity of the fluid). The limits on the diameter values prevent drastic changes in flow properties within a single flow block supporting our assumption of a Reynolds number based on average values. Here ϵ is the roughness of the internal surface of the channel. For our simulations, we assumed fairly smooth channels with surface roughness of $\epsilon \approx 1.5$ μm (drawn Cu tubing).

The heat transfer performance is modeled in terms of fluid temperatures at element boundaries and average temperature of the heated surface for each element. The energy balance for the fluid is given as:

$$\dot{m}C_{\mathrm{f}}\left(T_{\mathrm{f,out}} - T_{\mathrm{f,in}}\right) = h_{\mathrm{eff}}A\left(T_{\mathrm{s}} - \frac{T_{\mathrm{f,out}} + T_{\mathrm{f,in}}}{2}\right), \tag{5}$$

where C_{f} is the fluid specific heat, h_{eff} is the effective heat transfer coefficient between the fluid and heated surface temperature nodes, T_{s} is the temperature at the top surface which is subject to a uniform heat flux (q", Figure 1d) and $T_{\mathrm{f,in}}$, $T_{\mathrm{f,out}}$ are fluid inlet and outlet temperatures respectively. Overall heat transfer coefficient from the fluid to the top surface is obtained using:

$$\frac{1}{h_{\mathrm{eff}}A} = \frac{1}{hA_{\mathrm{c}}} + \frac{1}{k_{\mathrm{s}}S}, \tag{6}$$

where k_{s} is the thermal conductivity of the solid material and A_{c} and S are the curved internal channel area wetted by fluid and conduction shape factor for heat transfer from the surface to the channel internal wall, respectively. The shape factor correlations are obtained based on parametric

simulations conducted prior to simulation of the flow. Here, h is the heat transfer coefficient at the fluid-solid internal channel wall calculated using the following well-validated correlations [50]:

$$\mathrm{Nu} = 4\,, \qquad \text{Laminar} \qquad (7)$$

$$\mathrm{Nu} = 0.023\,\mathrm{Re}^{0.8}\mathrm{Pr}^{0.4}, \qquad \text{Turbulent} \qquad (8)$$

$$h = \frac{\mathrm{Nu}k_\mathrm{f}}{d}. \qquad (9)$$

where Nu is the Nusselt number based on the average hydraulic diameter (d), Pr is the fluid Prandtl Number, and k_f is the fluid thermal conductivity. Convective heat transfer in the fluid cannot be modelled with either constant heat flux or constant wall temperature boundary conditions. Hence, an average Nusselt number for flow in a circular channel with constant wall heat flux and constant wall temperature were chosen for the laminar flow regime.

Conduction within the solid domain is considered while solving for the heated surface temperature as:

$$\frac{k_\mathrm{s}A_\mathrm{l}}{L}\sum_{\text{intenal}}(T_\mathrm{s}-T_\mathrm{nb}) + h_\mathrm{amb}A_\mathrm{l}\sum_{\text{corner}}(T_\mathrm{s}-T_\mathrm{amb}) + \dot{m}C_\mathrm{f}\left(T_\mathrm{f,out}-T_\mathrm{f,in}\right) = q"A_\mathrm{top}\,, \qquad (10)$$

where $q"$ is the heat flux, h_amb is the heat transfer coefficients to ambient at corner elements, A_l, A_top are the lateral and top surface areas respectively. The block lateral surface area is assumed to be equal for all faces of the block in contact with neighboring elements or ambient. The bottom surface is assumed to be adiabatic. Here, T_nb and T_amb denote the neighboring element top surface and ambient temperatures. Effects of heat spreading (lateral block to block heat transfer) within the solid domain is considered within the heat conduction equation. Equations (5) and (10) result in a set of linear equations which are solved to obtain the fluid and heated surface temperature profiles for the entire cold plate.

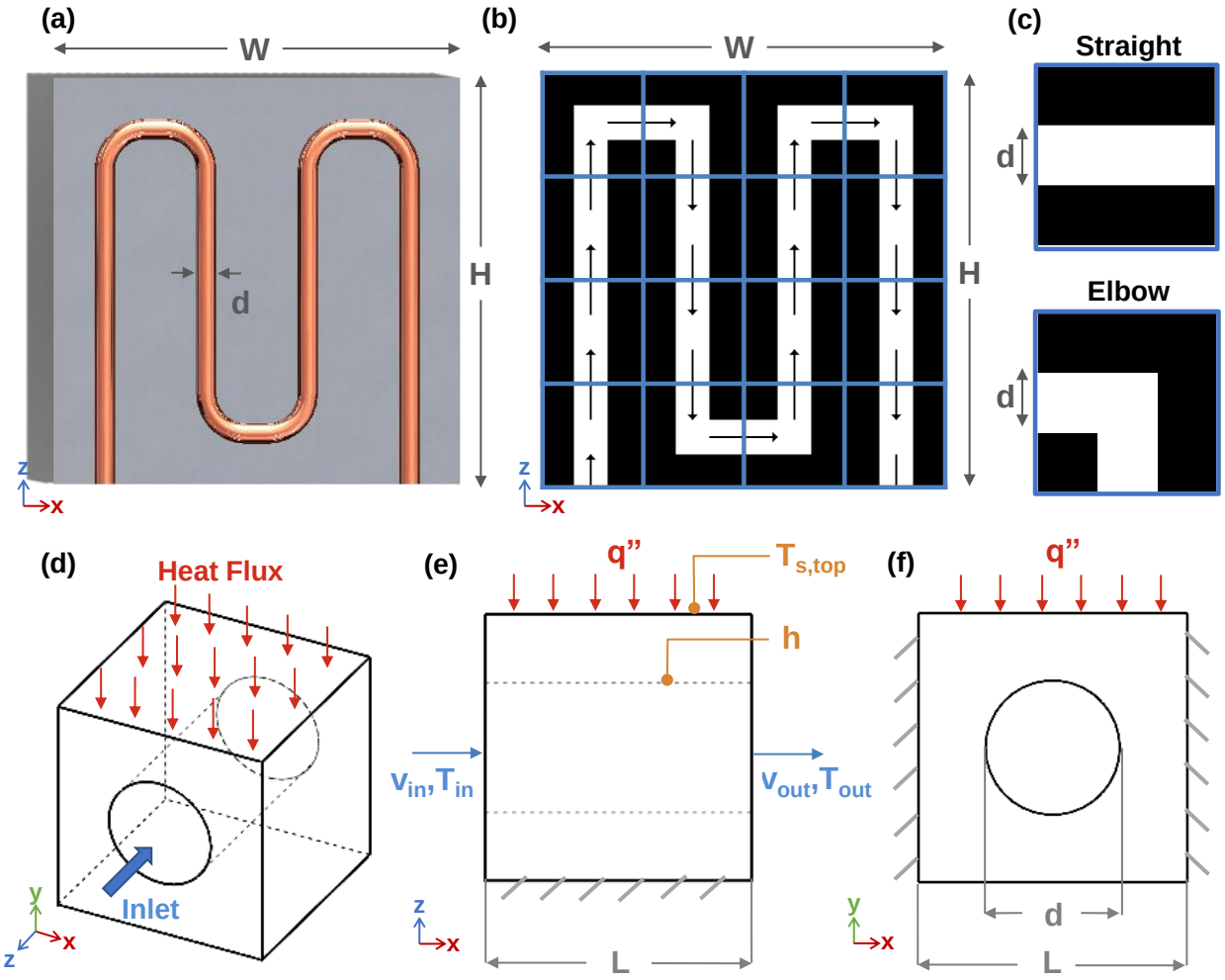

Figure 1. (a) Schematic of a commercial standard cold plate design for electronics cooling. (b) Top view of the cold plate domain divided into a coarse grid (blue divider lines) using (c) simplified flow blocks forming elements for cold plate design. Black arrows indicate flow direction, while black coloring represents the solid domain and white coloring represents the fluid domain. Schematics not to scale. (d) Schematic of a straight fluid block element (shown in Fig. 1c, top) with a heat flux boundary condition (q'' = constant) applied to the top surface (red arrows) and coolant entering through one circular face (blue arrow). (e) Side view of the fluid block showing the boundary conditions and flow and temperature variables including the inlet bulk fluid temperature (T_{in}) and average fluid velocity (v_{in}), along with the inner surface boundary condition of a fixed inner surface temperature (T_{s}) and inner local averaged heat transfer coefficient (h). (f) Front view of the fluid block indicating the inner tube diameter (d) and the fluid block element dimension (L). Hatched boundaries indicate adiabatic conditions (q'' = 0).

3. LAYOUT OPTIMIZATION

Dividing the flow path design into a set of building blocks allows for expressing the overall cold plate design in terms of a set of discrete variables. Each flow block is assigned a unique number identifying the type and direction of flow. Discrete optimization methods for maximizing the performance in terms of thermal-hydraulic parameters are explored. The design optimization consists of a multi-objective optimization problem which focuses on both thermal and hydraulic considerations. The optimization problem for minimizing thermal and hydraulic objectives can be formulated as:

$$\min_{\text{layout}} (T_{\text{s,max}}, \Delta P_{\text{tot}}, T_{\text{s,dev}}) \,, \tag{10}$$

subject to the following conditions:

$$\rho \text{v}_{\text{inlet}} A_{\text{inlet}} = \dot{m} \,, \tag{11}$$

$$q"(\text{i}, \text{j}) = q''_{\text{loss}} \,. \tag{12}$$

where min represents the multi-variable minimization function over the entire cold plate layout. Here, the maximum top surface temperature among all element blocks $T_{\text{s,max}}$, total pressure drop within entire channel ΔP_{tot} and the standard deviation of the top surface temperatures $T_{\text{s,dev}}$ are minimized with respect to the flow layout using the minimization function. The inlet mass flow rate $\dot{m}$ (Eq. 11) and local heat flux q''_{loss} at individual element locations (i, j, Eq. 12) form the optimization constraints. The multi-objective optimization of $T_{\text{s,max}}$, ΔP and $T_{\text{s,dev}}$ is solved using three unique approaches described herein.

Optimization Using a Genetic Algorithm

A Genetic Algorithm (GA) is a type of an evolutionary search algorithm [51]. The GA is effective for discrete optimization problems due to its heuristic search method which does not depend on gradient calculation [52]. The MATLAB-based *ga* function was applied for finding the optimal discrete design variables. We started by implementing the *ga* function to find the optimal design variables which correlated to the discrete flow block codes for all element locations. Each design variable represented an integer code for unique flow block type and flow direction at different grid locations.

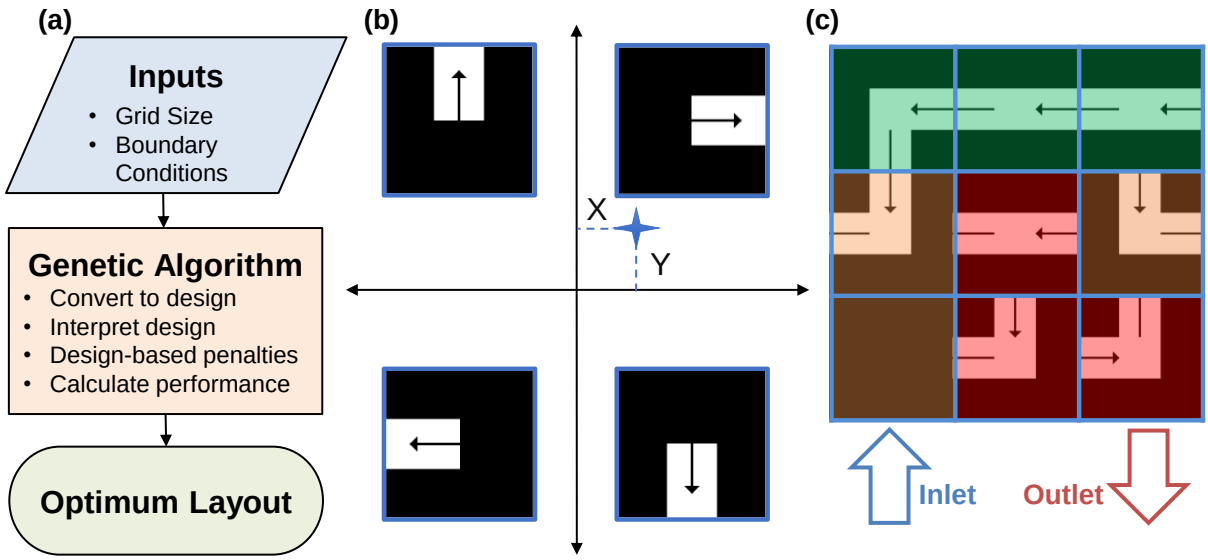

Figure 2. (a) Description of the layout optimization using the generic algorithm flow chart with a modified approach including continuous design variables and completeness-based penalties. (b) Method for implementing continuous design variables, each fluid block is represented in the form of two pairs of coordinates. The quadrant of the point represented by each pair indicates the direction of the flow for inlet and outlet in the fluid block. (c) Schematic of the penalization approach used for incomplete designs. The flow and temperature profiles are solved for incomplete designs by assigning weights favoring continuous elements (green color) while penalizing discontinuous elements (red color) and improper inlet/outlet assignments (orange color).

We assigned an arbitrary high value to the performance parameters being minimized for incomplete designs with partially connected flow layouts (Figure 2c). This direct implementation of the *ga* function for searching the optimal layout was unable to find a solution due to the limited feasible flow layouts in a large design space within a reasonable combination of the population size and number of iterations. We developed a modified objective function (Figure 2a) which incorporates encoding of designs in terms of continuous variables and penalizing incomplete designs to address this.

To express the design in terms of continuous variables, each flow block is modelled in terms of four variables incorporating two pairs of coordinates in a 2D number line (Figure 2b). The inlet and outlet flow direction for the block is determined based on the quadrant of the two variable pairs. This encoding approach correlates similar flow blocks which is not possible using the discrete representation. While obtaining the performance parameters for incomplete designs, penalty values are assigned based on different design characteristics (Figure 2c). Negative penalties are given for rewarding continuous chains of flow while positive penalties are given for having flow discontinuities as well as for having inlet/outlet ports at different grid elements from the preset locations. These modifications make the objective function behavior smoother in the design space and help identify optimal designs. The modified GA implementation was able to successfully find optimal layouts for a smaller grid size of 3 x 4 blocks with approximately 300 iterations of the solver with a population size of 1,000. The same approach however was unable to find a complete design solution for moderate grid sizes of 5 x 5, highlighting the main limitation of the GA-based layout optimization approach, thus inspiring the search for alternate methods.

Optimization using an Exhaustive Design Space Search

We were unable to perform layout optimization using the *ga* function because majority of variable combinations led to incomplete or non-feasible flow layouts. Given the limited number of feasible design layouts possible for a large design space, we considered an approach which relies on exhaustively searching for optimal performance within a set of feasible layouts (Figure 3a). We used path search algorithms [53] for finding feasible fluid flow paths connecting predefined inlet and outlet locations. In the process of finding all paths, we created a fringe for storing design nodes, defined as vectors with flow block codes at each element location. At each element location starting from the inlet, we added to the fringe nodes by finding all possible flow blocks that can be assigned (Figure 3b) based on the previous block. A node was terminated if the block assignment led to an already occupied location on the grid or found a boundary element other than the outlet location. Finally, a node leading to the outlet location was added to the set of feasible designs. The set of feasible designs was stored locally and is called for calculating performance given the boundary conditions for the layout optimization problem.

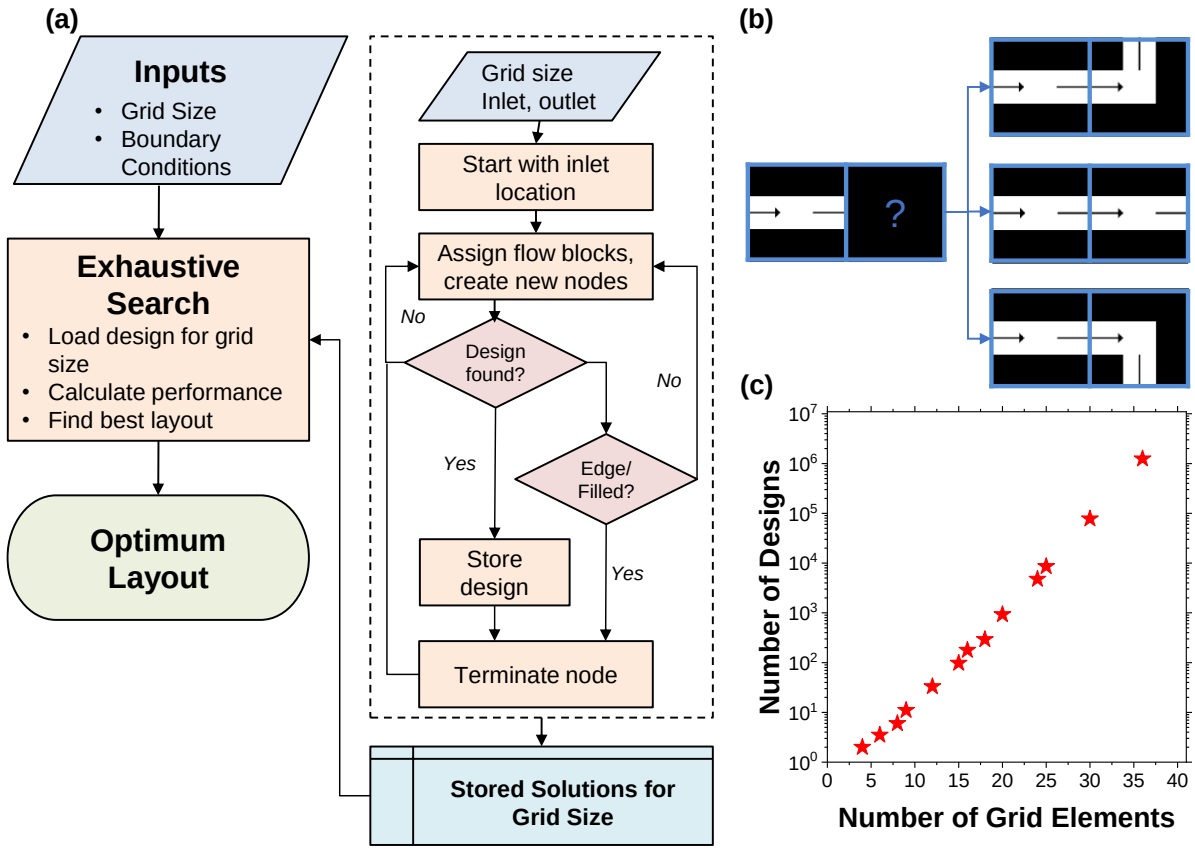

Figure 3. (a) Flow chart of the exhaustive design search method used for conducting the optimal layout exhaustive search (ES) within the design space. (b) Schematic showing an exemplary assignment of possible flow blocks to the next empty grid element. (c) Number of designs available as a function of the total number of fluid block elements (Figure 1).

Using the exhaustive design space search leads to optimization which ensures the best possible design. Even though the number of possible layouts is limited, the design space grows exponentially with the number of grid elements (Figure 3c). The requirements on runtime memory for maintaining the fringe with all design nodes and local memory for storing all possible layouts also increases significantly due to this exponential growth. For instance, the number of possible designs for a 3 x 4 grid size is 38 while that for a 6 x 6 grid size is 1,246,850. The time required

for calculating the performance metrics for each unique heat dissipation profile for all possible designs is another detrimental factor against using this approach.

Optimization using an Optimal Path Search

The previous two approaches were incapable in meeting the requirements for rapid layout optimization. An approach building on the merits of the last two approaches is discussed herein. The advantages offered by the heuristic search nature of the discrete optimization methods and ease of finding feasible layouts using the path search method were combined in this approach (Figure 4a).

Figure 4b shows the flow layout formed by the shortest path starting from the inlet, connecting a series of control points leading to the outlet. We used a heuristic search method [53] to find the shortest path on a partially filled grid using the Manhattan distance between the current location and the next control point location as the heuristic. The process of connecting shortest path through control points is repeated for a randomized population of control points. Performance parameters are calculated and compared for each of the generated designs. Progressively increasing the number of control points on the grid and randomized population search increased the possibility of finding the optimal solution using this approach for any given combination of boundary conditions. A smaller number of control points usually led to shorter designs which are desirable for having low pressure drop. Conversely, a greater number of control points ensures that the fluid reaches all heat dissipation locations with favorable thermal performance. Several designs analyzed can be used to find not only a single optimal layout, but a series of Pareto optimal layouts for the multi-objective optimization problem.

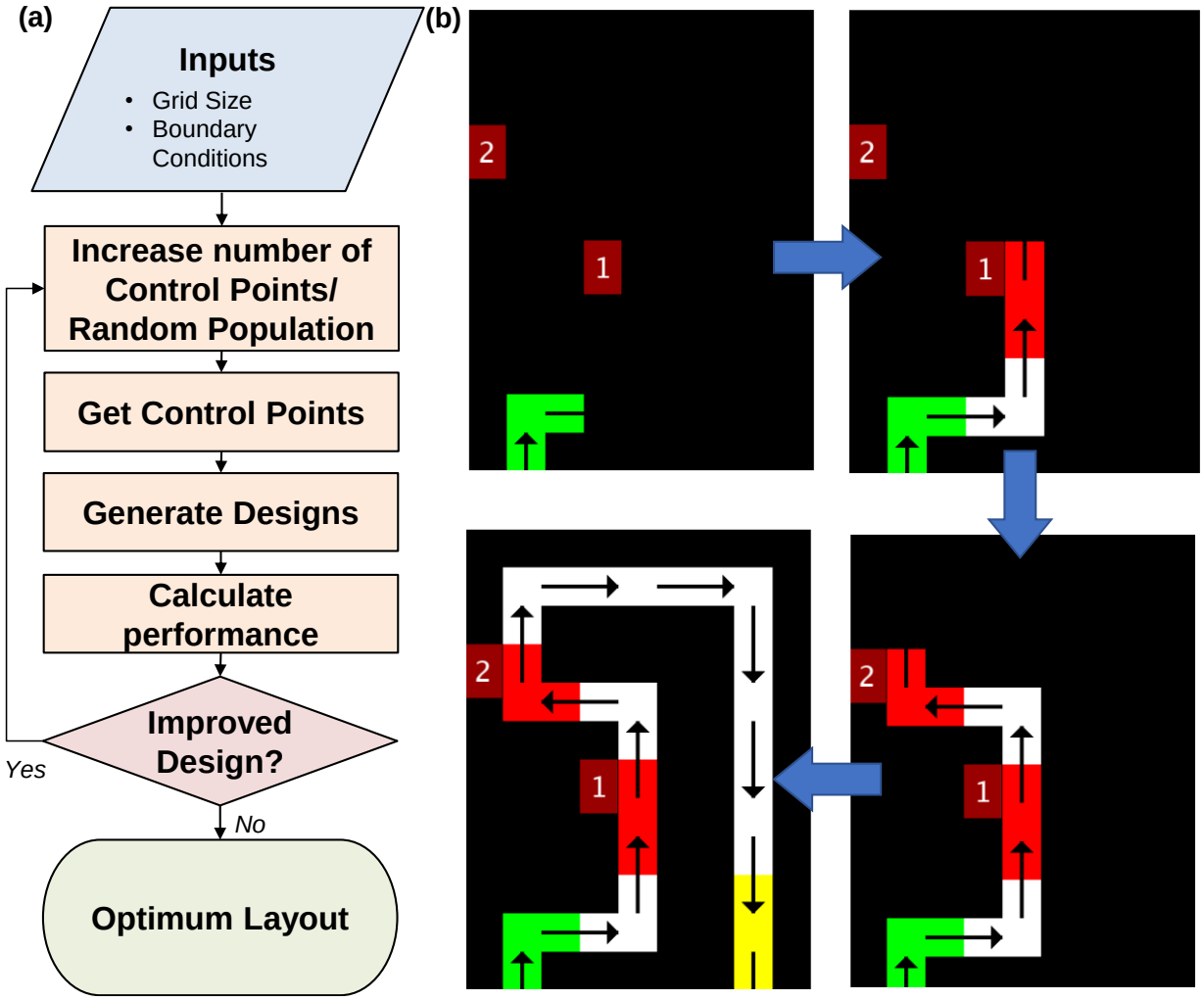

Figure 4. (a) Flow chart of the optimal path search (OPS) layout optimization approach for a fixed grid size and set of boundary conditions. A set of control points with randomized locations on the grid are selected. A design is generated for each of these locations using the shortest path approach (Fig. 4a,b). For all solutions, performance metrics are calculated. (b) Exemplary design search connecting inlet and outlet locations going through the shortest path including highlighted control points (1 and 2) on the grid. Blue arrows indicate sequential steps in the search. This process is repeated with a number of randomized control points in the OPS layout optimization approach.

The optimal path search (OPS) approach successfully identified the Pareto front for the bi-objective optimization of thermal resistance and pressure drop shown in Figure 5. Optimization was carried out for grid sizes of 4 x 4, 5 x 5 and 6 x 6 for a design having the same overall dimensions with equivalent boundary conditions. The Pareto fronts were obtained using a number of control points ranging from 2 to 24 (depending on grid size) each with 500 randomized sets of

control points. As seen from the results (Fig. 5), for the same design, higher grid size results in smaller block dimensions and thus overall higher pressure drop. Thermal performance improves with increasing grid size with minimum temperatures of 79.8ºC for 4 x 4, 64.6ºC for 5 x 5 and 54.5ºC for the 6 x 6 grid size. As the grid size increases, the maximum $T_{s,max}$ which corresponds to the shortest path connecting the inlet and outlet port locations (simple path connecting the first row of elements on the coarse grid) increases. The increase is due to the lower portion of the total area covered by the fluid path for higher grid sizes. The overall minimum pressure drop which corresponds to these designs also decreases showing that the Pareto front improves with respect to both design variables individually with increase in the grid size.

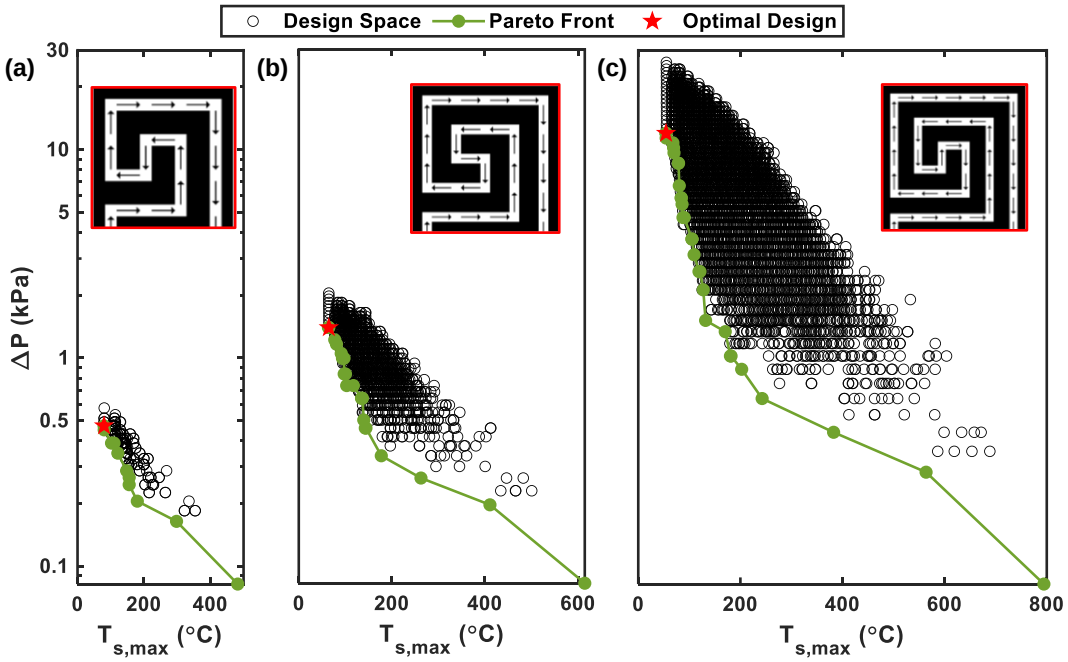

Figure 5. Design space representing the cold plate pressure drop and maximum temperature for all designs (black circles) along with the Pareto frontier (green points) obtained using the OPS approach with an (a) 4 x 4 grid: 178 designs, (b) 5 x 5 grid: 8,591 designs, and (c) 6 x 6 grid: 1,246,850 designs. The green line connecting the Pareto front is a trend line. Inset images: optimal design for thermal performance based on the grid arrangement for each individual OPS search.

Figure 6 shows the effects of different boundary conditions and design constraints on optimal layouts obtained using the OPS method. For a grid size of 4 x 4, the effect of two heat

dissipation profiles including uniform and concentrated profiles was considered (Figures 6a, b). For the uniform loss profile, all grid elements were assigned a fixed heat dissipation value of 200 W (q'' = 50 W/cm^2). In the concentrated loss case, the four central grid elements were assigned a fixed heat dissipation value of 800 W (q'' = 200 W/cm^2), with all other elements being adiabatic (q'' = 0) ensuring that the total heat dissipation in both cases is identical. The pressure drop for both uniform and concentrated heat dissipation cases is constrained at a value of ΔP = 0.81 kPa for an inlet mass flow rate of 0.1 kg/s with water as coolant. Aluminum is considered as the solid domain material. The fluid block height is L = 2 cm and diameter values for all blocks are d = 1.5 cm. The Pareto-optimal layouts identified by the OPS differ for the two loss profiles. The uniform heat dissipation profile design connects dispersed points on the grid while the concentrated loss profile design covers all of the central location. Moreover, the maximum top surface temperature among all elements with uniform loss is 130.2ºC with Design 1 which is originally optimized for uniform heat dissipation (Figure 6a) and 166.3ºC with Design 2 which is optimized for concentrated heat dissipation (Figure 6b). The maximum surface temperature in the case of concentrated loss with Design 1 is 194.2ºC while that for Design 2 is 151.2ºC. Both designs perform better with the heat dissipation profile for which they are optimized for. Allowing the inlet and outlet elements to change positions can lead to further improvement in the optimal designs (Figures 6c, d). For this, we carried out the design optimization analysis for a grid size of 5 x 5 having flow conditions and individual block dimensions same as before. The Pareto front shifts to the left (lower maximum surface temperature) when the inlet/outlet locations are allowed to float and are not fixed at the bottom side of the cold plate, indicating that better Pareto optimal performance is possible. Fixed inlet/outlet port locations serve as additional constraints, the

removal of which acts to increase the number of possible layouts which can generate better thermal-hydraulic performance.

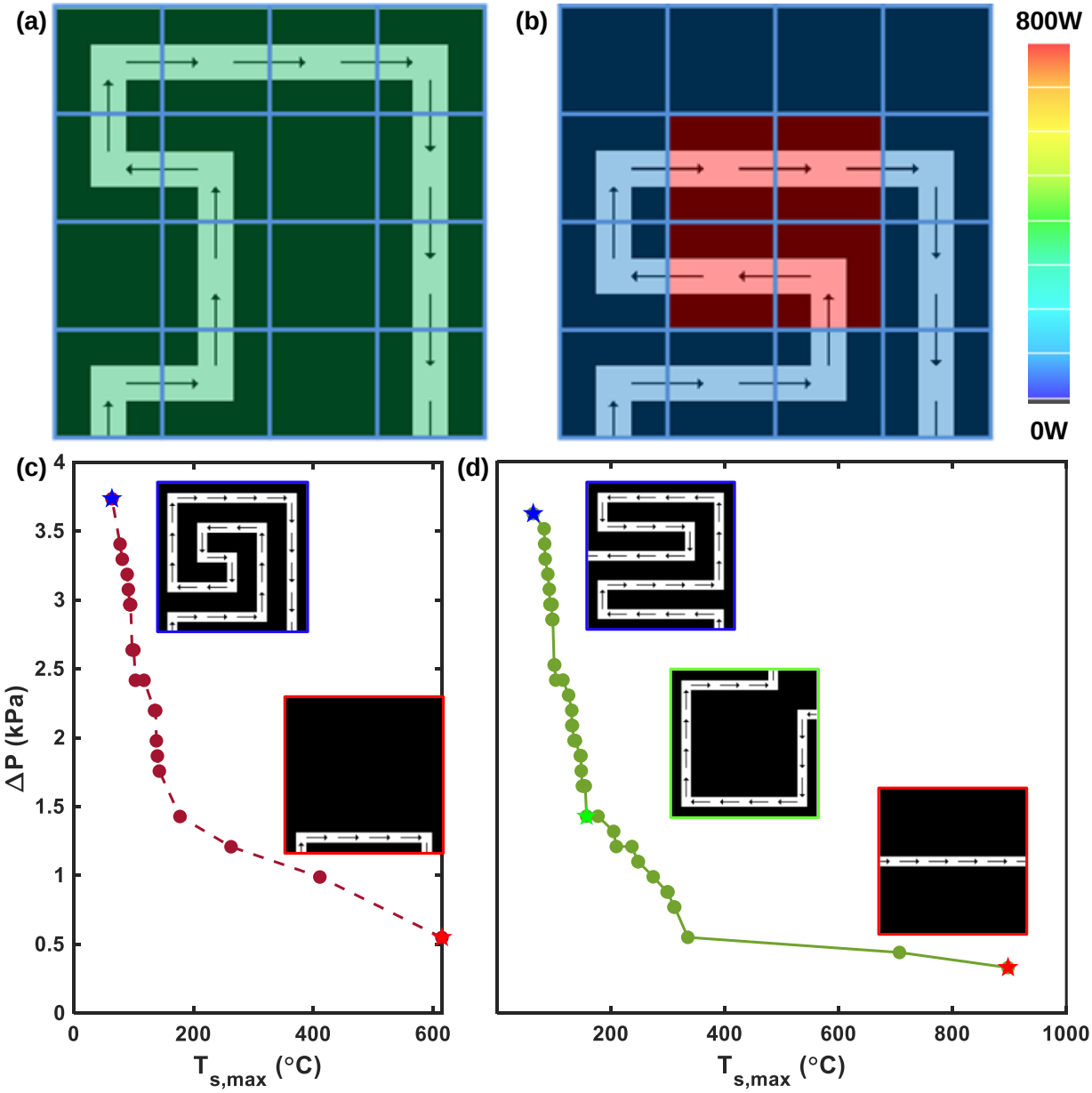

Figure 6. Optimal design layout change as a function of input conditions: (a) optimal layout generated for uniform heat dissipation case on 4 x 4 grid with 200 W loss for each element (b) optimal layout for concentrated heat dissipation with 800W on four central elements and zero loss on corner elements (c) Pareto front for 5 x 5 grid size with fixed inlet at bottom left and outlet at bottom right corner of the design (d) pareto front for the case with flexible inlet/outlet locations, inset images in (c) and (d) show pareto optimal designs in both cases.

4. CROSS-SECTION GEOMETRY OPTIMIZATION

We carried out optimization of the cross-section geometrical parameters after obtaining the optimal flow layout for a given grid size and boundary condition. The optimization formulation for the cross-section geometry is similar to Eq. (5) with diameter values for the flow blocks now representing design variables instead of the 2D flow layout. We note that the geometry optimization described herein is not only a part of the overall design optimization but can also independently serve as a design improvement tool for maximizing performance for a set 2D layout.

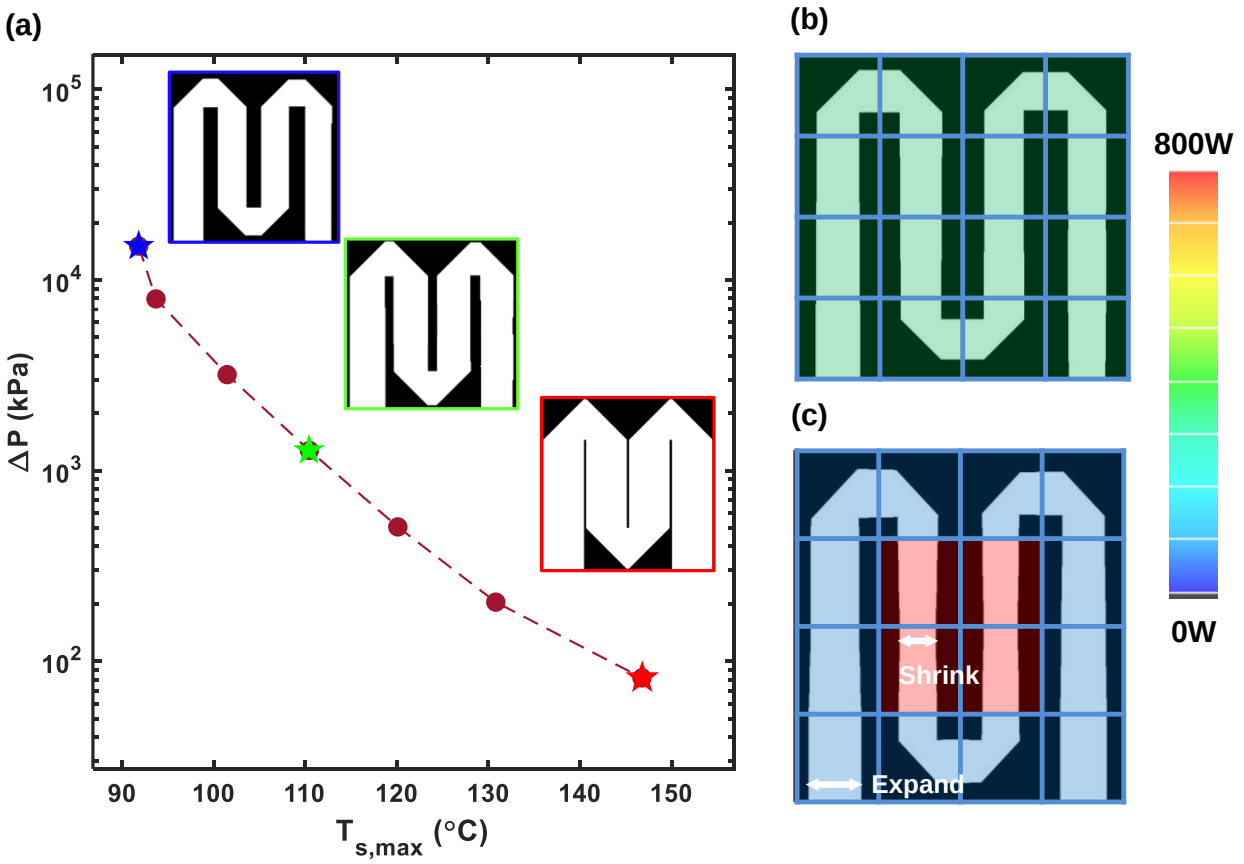

Figure 7. Results of geometry optimization: (a) pareto front for bi-objective optimization of maximum surface temperature ($T_{s,max}$) and pressure drop (ΔP) using optimization of geometrical parameters (fluid flow block diameters), geometry optimized design for (b) uniform heat dissipation profile with 200W per element and (c) concentrated heat dissipation with 800W on four central elements and zero loss on corner elements.

The objectives and constraints for geometry optimization are continuous functions of the design variables (diameters, d). We can use gradient-based optimization which converges faster to local optima as compared to methods such as the GA. Here, we use the MATLAB *fmincon* function for geometry optimization. Figure 7 highlights results of geometry optimization for a given flow layout in different cases. Figure 7a shows a set of Pareto optimal points for thermal-hydraulic bi-objective optimization obtained using optimization of the channel diameters. The insets in the plot show optimal designs for different combinations of thermal resistance and pressure drop objectives. On the pareto front, designs with higher weightage to pressure drop objectives have larger channel diameters, because pressure drop increases for lower channel diameters. Designs with higher weightage to thermal resistance objective have lower diameters since the heat transfer coefficient is inversely proportional to the hydraulic diameter.

We studied the effect of heat dissipation profile on optimal diameters with uniform and concentrated profiles. Once again, the uniform heat dissipation profile assumes equal heat flux on all element faces while the concentrated profile assumes heat flux only on the four central elements, with equal total loss in both cases. In the case of uniform heat dissipation (Figure 7b), the optimal diameter values are nearly equal for all element faces, resulting in low pressure drop encountered for the gradual changes in diameters. For the concentrated heat dissipation profile (Figure 7c), the diameter values in the central region where heat dissipations are applied are smaller than the uniform heat dissipation case. The smaller diameters lead to increased local heat transfer coefficients, and also cause higher pressure drop. To counter the elevated pressure drop while maintaining good thermal performance, the optimal design selects larger diameter values in the outer regions of the grid near the edges, with the resulting total pressure drop being similar for both the uniform and concentrated heat dissipation cases.

5. OVERALL DESIGN OPTIMIZATION

Figure 8 shows a design optimization framework that integrates layout optimization and cross-section geometry optimization. The input for the design optimization problem is obtained as a 2D schematic of the electronic system with locations specified for heat generating devices. The layout is then transformed into a coarse grid, with the device locations translated to the grid element with specified heat dissipation. First, the optimal layout search is carried out using OPS, using the heat transfer and flow boundary conditions. A design is chosen from the Pareto-optimal points to get the desired trade-off between thermal and hydraulic objectives. Second, geometry optimization is performed on the flow layout obtained in the previous step. For the geometry optimization step, the pressure drop with the design obtained from layout optimization is used as a constraint to minimize the thermal objective.

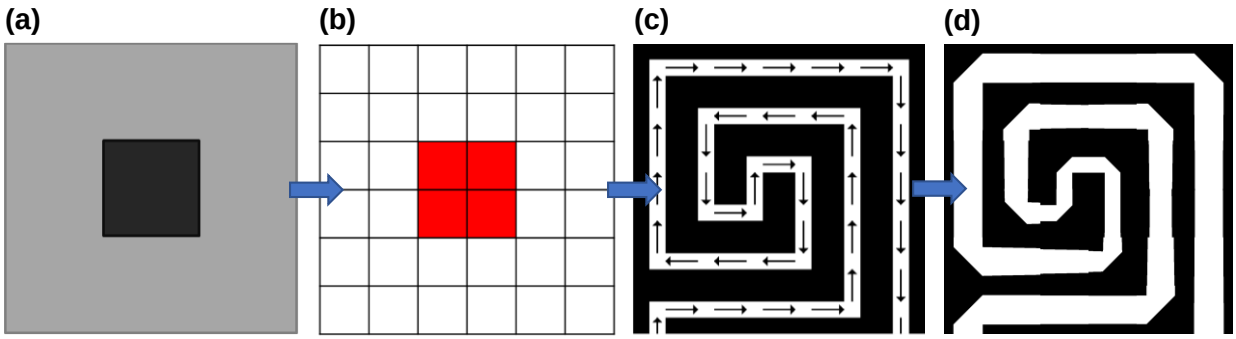

Figure 8. Design optimization process: (a) input problem defining heterogeneous loss, (b) capture of design domain and heat dissipation profile, (c) layout optimization based on grid size and boundary conditions to optimize thermal-hydraulic performance followed by (d) optimization of thermal metrics with hydraulic performance (pressure drop) of optimal layout as a constraint with respect to geometrical parameters.

Power Module Case Study

Figure 9 shows a case study applying the design optimization method for single-phase liquid cooling of electronics. The study targets an XM3 series half-bridge module developed by Wolfspeed (Figure 9a) [54,55]. The XM3 series power modules are developed for electric vehicle (EV) chargers and traction drives. The module packaging includes discrete Silicon Carbide (SiC) semiconductor devices which act as the major heat generating sources with a Silicon Nitride (SiN) substrate and a copper (Cu) base plate for heat spreading. A region within the geometry of the module is divided into a coarse grid (Figure 9b) of 9 x 4 blocks for design optimization.

First, we obtained the optimal layout for the given set of input parameters using the OPS approach (Figure 9c) to minimize thermal resistance. Second, the cross-section geometry optimization was used to generate the diameter values to further minimize thermal resistance with constrained pressure drop (Figure 9d). We built three-dimensional (3D) CAD models for the layout (Figure 9f) and geometry optimized (Figure 9g) designs using Autodesk Fusion360. Finally, we mapped the performance of the two designs using 3D CFD simulations in COMSOL Multiphysics (version 5.6). We performed simulations for a total heat dissipation of 500 W distributed among the devices (Figure 9e). This heat loss corresponds to a local device-level heat flux of 178.5 W/cm2 as computed using the device base area. Considering the effect of heat spreading from device to base plate, the heat flux was reduced to an average of 62.5 W/cm2 due to the larger area of the base plate. We considered Water-Ethylene Glycol mixture (50% by volume) as the coolant for total flow rates ranging from 2 to 8 LPM with a bulk coolant inlet temperature of 25°C. WEG was chosen as a preferred coolant due to its use in electric vehicle (EV) and hybrid electric vehicle (HEV) onboard cooling systems due to its lower freezing points when compared to water. We chose WEG50 as our coolant for analysis in order to recreate conditions similar to the ones used

in reported SOA cold plate performance metrics which are available for comparison. The cold plate material was assumed to be Aluminum alloy. A Thermal Interface Material (TIM) layer was included between heatsink and module baseplate having a 100 µm thickness and a 5 W/(m·K) thermal conductivity.

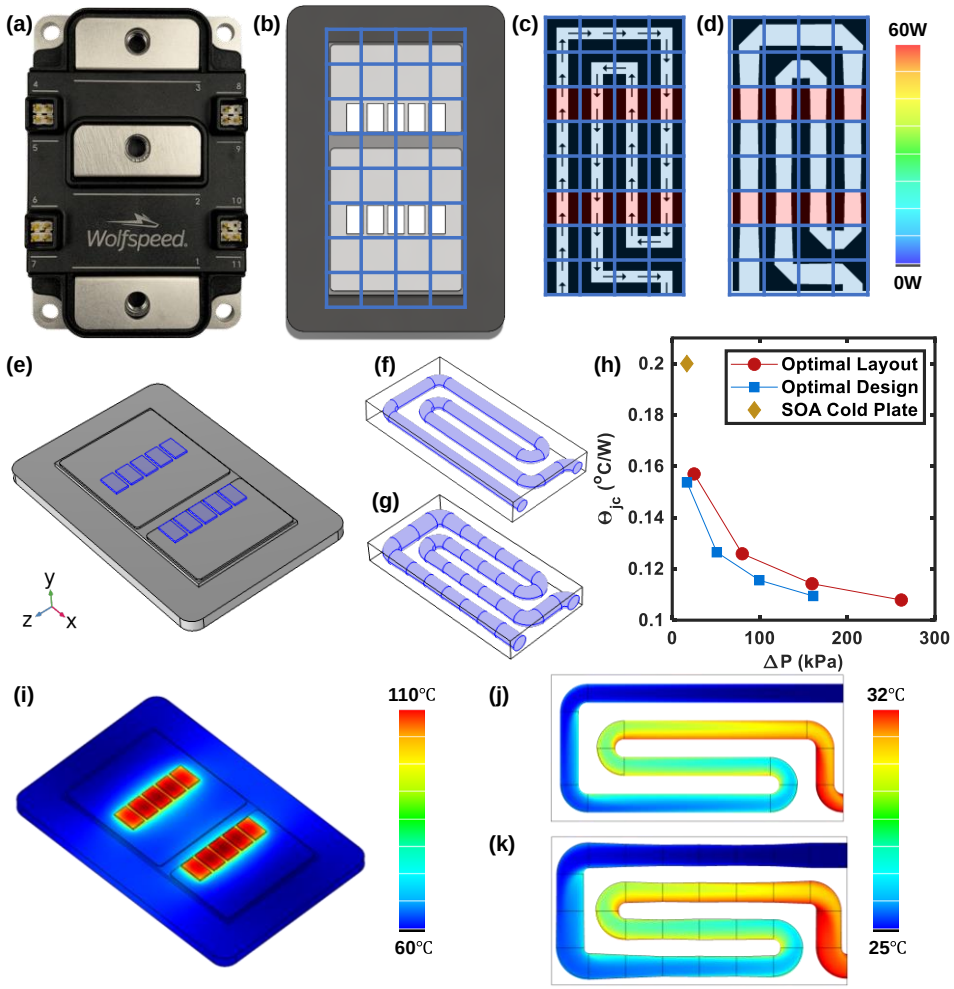

Figure 9. Case study with cold plate designer: (a) Wolf Speed XM3 half-bridge power module (b) Top view of module with coarse grid for design optimization (c) designs with optimal layout search using OPS and (d) geometry optimization (e) Simulation setup for XM3 cooling simulation with highlighted loss locations, 3D schematic of fluid flow domains for (f) layout optimized design and (g) geometry optimized design, (h) junction-to-coolant thermal resistance (Θ_{jc}) as a function of pressure drop (ΔP) for the two design cases along with state-of-the-art (SOA) cold plate (Wieland Microcool CP4012). (i) Temperature profile of the XM3 power module obtained from the simulation results. Fluid domain temperature profile for the (j) layout optimized and (k) geometry optimized designs.

We carried out preliminary simulations for multiple mesh densities including 0.71, 3.04, 9.48 and 16.01 million elements to check for mesh independence. Results showed < 2% change in both maximum temperature and pressure drop for the three higher mesh densities. Based on this result, we chose a mesh density corresponding to 3.04 million elements considering both simulation accuracy and computational expense for further simulations. We obtained the junction-to-coolant thermal resistance which is the ratio of the difference between the maximum SiC device junction and coolant temperatures to total heat dissipation along with total cold plate pressure drop (Figure 9h). The design with both optimum layout and geometry outperforms the design having only the optimum layout with an average 4.5% reduction in the junction-to-coolant thermal resistance for a given pressure drop over the range of flow rates considered. Figure 9(h) shows a comparison between the optimal cold plate and a state-of-the-art (SOA) cold plate developed by Wieland Microcool (CP4012) specifically for cooling of XM3 power modules. The SOA cold plate has higher thermal resistance (0.2ºC/W) [55] for a comparable value of pressure drop when compared to the optimal design (0.15ºC/W), demonstrating a 25% reduction at approximately 16 kPa pressure drop.

6. DISCUSSION

We developed a rapid design optimization tool for single phase liquid cooled heat sinks such as cold plates and microchannel coolers used in electronics cooling. Using our method, optimized solutions were typically obtained within at a time scale of 60-120 s depending on the design complexity and grid size. Here, we used serial computing for performing all computations with the aim of developing a simple software tool for reduced order optimization. Parallel computing can be employed in future work for several functions including layout search on randomized

populations [56], which will further reduce time required for finding optimal designs. We used a modeling approach that predicts thermal-hydraulic performance on a coarse grid resulting in low computational effort. Although the key assumptions made to develop our simplified modeling approach can result in lower-fidelity estimation of thermal-hydraulic parameters, comparative performance of designs under investigation can be expected to be the same as that obtained using high-fidelity simulation methods. This enables the use of reduced order modeling for design optimization. Despite the non-optimal prediction fidelity, modeling accuracy can be further improved with the incorporation of correlations developed for flow and temperature parameters using high fidelity CFD simulations.

Flow layout can have a significant impact on cooling performance [28–34]. A layout optimization sub-module was developed to find flow route extracting maximum thermal performance while maintaining low pressure drop. Discrete search and optimization techniques were explored to develop a method for finding the flow layout that optimizes the thermal-hydraulic performance. An approach relying on the advantages of the path-finding algorithm and a population-based search was realized in the form of the OPS approach. Combining the heuristic nature of GA with the assurance of finding a complete layout with path search algorithms, our OPS approach enables a rapid layout search. Even though the OPS approach is able to capture layouts performing better than alternatives for most cases, it does not guarantee an optimal solution as evident from the missed Pareto optimal points while generating the Pareto front. The chances of finding an optimum could be improved by increasing the number of search points (granularity of the fundamental design elements) at the cost of increased time requirement to conduct the search and estimate thermal-hydraulic performance.

Our work focuses on designs with non-splitting flow layouts (serial channels). Dedicated correlations to differentiate the flow behavior and resulting thermal performance changes in elbows as compared to straight blocks are required. Furthermore, additional development is needed to establish a performance modeling approach that can include flow branching. In addition, the method should be modified to accommodate non-uniform grids to allow local refinement within the cold plate geometry. Layout search and geometry optimization methods also need to be modified to consider parallel flow architectures. Similar to the simple flow blocks used in this work, correlations can be developed for blocks including performance enhancing aspects such as internal fins and turbulence inducing features. Advanced manufacturing methods including additive manufacturing can make such designs realizable [57–62]. In the future, it would be interesting to utilize our tool to conduct additional case studies for practical cooling applications with differing heat dissipation profiles and compare the results with the well-established cooling methods currently used [63]. Furthermore, future work is needed to obtain rigorous design optimization performance benchmarks against state-of-the-art design methods and design optimization software packages (ANSYS, COMSOL) in the context of required computational resources and timescale for identification of an optimal solution.

Two-phase heat sinks for cooling of electronics are a topic of high interest. Flow boiling in channel flow offers potential for achieving higher heat flux removal capabilities when compared to single-phase liquid flow while also providing isothermal cooling [64–66]. The coarse meshing approach for performance prediction presented in this work can be translated for heat sinks undergoing two-phase flow without impacting the computational speeds. This can be achieved with reliable correlations which are available for predicting macro-scale flow and thermal

behavior. Reliability of such applications of the tool needs to be validated and improved with the help of high-fidelity simulations [67–69] and experimental approaches [70–72].

Rapid design optimization creates potential for integration with electro-thermal co-design tools already available [2–5]. Traditional approaches mainly rely on detailed thermal analysis based on numerical methods requiring significant time and computational effort. These approaches limit the number of design iterations available for identifying the optimal packaging of electronics. These also require a level of user expertise in setting up the numerical simulations to ensure accurate results. The methods demonstrated in this work allow for the rapid design of compact electronics packaging systems with high performance cooling solutions. The designs generated using this method can also be used as starting points for high fidelity design optimization using TO.

7. CONCLUSIONS

We demonstrate that design of single-phase liquid cooled channel heat sinks can be optimized using limited time and computing resources. Our approach combines modeling on a coarse grid using existing performance correlations for obtaining pressure drop and temperature profiles, flow layout optimization through multiple path searches using randomized populations and gradient-based optimization for cross-section geometries. The reduced-order nature of this method offers significant benefits in terms of computational and temporal requirements when compared to traditional design optimization methods using CFD simulations coupled with numerical optimization. We show the ability of the developed method to address heterogeneous loss profiles commonly seen in electronics packaging. We conducted a case study demonstrating the application of the developed design optimization method for a commercial XM3 power electronics module.

The results indicate a potential reduction of 25% in junction-to-coolant thermal resistance compared to an aggressive state-of-the-art cooling solution. The design tool enables the versatile incorporation of enhancements such as consideration of parallel flow designs, two-phase flows, internal flow features (fins), and non-uniform grids. The rapid solution and low computational requirement of the developed tool enable potential design application in electro-thermal co-design for electronics packaging.

ACKNOWLEDGMENTS

The authors thank Professor James Allison, Dr. Satya Ravi Teja Peddada, Cary Laird for their support with the channel area optimization model. The authors also thank Professors Mehdi Asheghi and Kenneth Goodson of Stanford University for useful discussions regarding thermal-hydraulic considerations and modeling. The authors also gratefully acknowledge funding for this work in part from the Power Optimization of Electro-Thermal Systems (POETS) National Science Foundation Engineering Research Center with cooperative agreement EEC-1449548, and the International Institute for Carbon Neutral Energy Research (WPI-I2CNER), sponsored by the Japanese Ministry of Education, Culture, Sports, Science and Technology.

REFERENCES

[1] Hoefflinger, B., 2011, "ITRS: The International Technology Roadmap for Semiconductors," Springer, Berlin, Heidelberg, pp. 161–174.

[2] Park, Y., Yuruker, S., Chakraborty, S., Khaligh, A., Mandel, R., McCluskey, P., Ohadi, M., Boteler, L., and Hinojosa, M., 2020, "Electro-Thermal Co-Design of a Cooling System-Integrated High-Frequency Transformer," *2020 IEEE Transportation Electrification Conference and Expo, ITEC 2020*, Institute of Electrical and Electronics Engineers Inc., pp. 26–31.

[3] Deckard, M., Shamberger, P., Fish, M., Berman, M., Wang, J., and Boteler, L., 2019, "Convergence and Validation in Parapower: A Design Tool for Phase Change Materials in Electronics Packaging," *InterSociety Conference on Thermal and Thermomechanical Phenomena in Electronic Systems, ITHERM*, IEEE Computer Society, pp. 878–885.

[4] Razi, A., Le, Q., Evans, T. M., Mukherjee, S., Mantooth, H. A., and Peng, Y., 2021, "PowerSynth Design Automation Flow for Hierarchical and Heterogeneous 2.5-D Multichip Power Modules," IEEE TRANSACTIONS ON POWER ELECTRONICS, **36**(8).

[5] Mademlis, G., Orbay, R., Liu, Y., Sharma, N., Arvidsson, R., and Thiringer, T., 2021, "Multidisciplinary Cooling Design Tool for Electric Vehicle SiC Inverters Utilizing Transient 3D-CFD Computations," eTransportation, **7**, p. 100092.

[6] Frank P. Incorprera, 1999, "Liquid Cooling of Electronic Devices by Single-Phase Convection," 978-0-471-15986-5, John Wiley & Sons, Inc., Hoboken, New Jersey, the United States [Online]. Available: https://www.wiley.com/en-

us/Liquid+Cooling+of+Electronic+Devices+by+Single+Phase+Convection-p-9780471159865. [Accessed: 12-Jun-2021].

[7] Joshi, Y., and Wan, Z., 2017, "Single- and Multiphase Flow for Electronic Cooling," *Handbook of Thermal Science and Engineering*, Springer International Publishing, pp. 1–58.

[8] Iradukunda, A. C., Huitink, D. R., and Luo, F., 2020, "A Review of Advanced Thermal Management Solutions and the Implications for Integration in High-Voltage Packages," IEEE Journal of Emerging and Selected Topics in Power Electronics, **8**(1), pp. 256–271.

[9] Tuckerman, D. B., and Pease, R. F. W., 1981, "High-Performance Heat Sinking for VLSI," IEEE Electron Device Letters, **EDL-2**(5), pp. 126–129.

[10] Weisberg, A., Bau, H. H., and Zemel, J. N., 1992, "Analysis of Microchannels for Integrated Cooling," International Journal of Heat and Mass Transfer, **35**(10), pp. 2465–2474.

[11] Peng, X. F., and Peterson, G. P., 1995, "The Effect of Thermofluid and Geometrical Parameters on Convection of Liquids through Rectangular Microchannels," International Journal of Heat and Mass Transfer, **38**(4), pp. 755–758.

[12] Qu, W., and Mudawar, I., 2002, "Experimental and Numerical Study of Pressure Drop and Heat Transfer in a Single-Phase Micro-Channel Heat Sink," International Journal of Heat and Mass Transfer, **45**(12), pp. 2549–2565.

[13] Knight, R. W., Goodling, J. S., and Hall, D. J., 1991, "Optimal Thermal Design of Forced Conwection Heat Sinks-Analytical," Journal of Electronic Packaging, Transactions of the ASME, **113**(3), pp. 313–321.

[14] Kim, S. J., and Kim, D., 1999, "Forced Convection in Microstructures for Electronic Equipment Cooling," Journal of Heat Transfer, **121**(3), pp. 639–645.

[15] Zhao, C. Y., and Lu, T. J., 2002, "Analysis of Microchannel Heat Sinks for Electronics Cooling," International Journal of Heat and Mass Transfer, **45**(24), pp. 4857–4869.

[16] Chen, C. H., 2007, "Forced Convection Heat Transfer in Microchannel Heat Sinks," International Journal of Heat and Mass Transfer, **50**(11–12), pp. 2182–2189.

[17] Xie, X. L., Liu, Z. J., He, Y. L., and Tao, W. Q., 2009, "Numerical Study of Laminar Heat Transfer and Pressure Drop Characteristics in a Water-Cooled Minichannel Heat Sink," Applied Thermal Engineering, **29**(1), pp. 64–74.

[18] Xie, X. L., Tao, W. Q., and He, Y. L., 2007, "Numerical Study of Turbulent Heat Transfer and Pressure Drop Characteristics in a Water-Cooled Minichannel Heat Sink," Journal of Electronic Packaging, Transactions of the ASME, **129**(3), pp. 247–255.

[19] Fedorov, A. G., and Viskanta, R., 2000, "Three-Dimensional Conjugate Heat Transfer in the Microchannel Heat Sink for Electronic Packaging," International Journal of Heat and Mass Transfer, **43**(3), pp. 399–415.

[20] Chai, L., Xia, G. D., and Wang, H. S., 2016, "Parametric Study on Thermal and Hydraulic Characteristics of Laminar Flow in Microchannel Heat Sink with Fan-Shaped Ribs on Sidewalls - Part 1: Heat Transfer," International Journal of Heat and Mass Transfer, **97**, pp. 1069–1080.

[21] Chai, L., Xia, G. D., and Wang, H. S., 2016, "Parametric Study on Thermal and Hydraulic Characteristics of Laminar Flow in Microchannel Heat Sink with Fan-Shaped Ribs on Sidewalls - Part 2: Pressure Drop," International Journal of Heat and Mass Transfer, **97**, pp. 1081–1090.

[22] Chai, L., Xia, G. D., and Wang, H. S., 2016, "Parametric Study on Thermal and Hydraulic Characteristics of Laminar Flow in Microchannel Heat Sink with Fan-Shaped Ribs on

Sidewalls - Part 3: Performance Evaluation," International Journal of Heat and Mass Transfer, **97**, pp. 1091–1101.

[23] Knight, R. W., Goodling, J. S., Hall, D. J., and Jaeger, R. C., 1992, "Heat Sink Optimization with Application to Microchannels," IEEE Transactions on Components, Hybrids, and Manufacturing Technology, **15**(5), pp. 832–842.

[24] Murakami, Y., and Mikić, B. B., 2001, "Parametric Optimization of Multichanneled Heat Sinks for VLSI Chip Cooling," IEEE Transactions on Components and Packaging Technologies, **24**(1), pp. 2–9.

[25] Sharma, C. S., Zimmermann, S., Tiwari, M. K., Michel, B., and Poulikakos, D., 2012, "Optimal Thermal Operation of Liquid-Cooled Electronic Chips," International Journal of Heat and Mass Transfer, **55**(7–8), pp. 1957–1969.

[26] Zhang, J., Lin, P. T., and Jaluria, Y., 2014, "Design and Optimization of Multiple Microchannel Heat Transfer Systems," Journal of Thermal Science and Engineering Applications, **6**(1).

[27] Hadad, Y., Ramakrishnan, B., Pejman, R., Rangarajan, S., Chiarot, P. R., Pattamatta, A., and Sammakia, B., 2019, "Three-Objective Shape Optimization and Parametric Study of a Micro-Channel Heat Sink with Discrete Non-Uniform Heat Flux Boundary Conditions."

[28] Sui, Y., Teo, C. J., Lee, P. S., Chew, Y. T., and Shu, C., 2010, "Fluid Flow and Heat Transfer in Wavy Microchannels," International Journal of Heat and Mass Transfer, **53**(13–14), pp. 2760–2772.

[29] Sui, Y., Lee, P. S., and Teo, C. J., 2011, "An Experimental Study of Flow Friction and Heat Transfer in Wavy Microchannels with Rectangular Cross Section," International Journal of Thermal Sciences, **50**(12), pp. 2473–2482.

[30] Xie, G., Liu, J., Zhang, W., and Sunden, B., 2012, "Analysis of Flow and Thermal Performance of a Water-Cooled Transversal Wavy Microchannel Heat Sink for Chip Cooling," Journal of Electronic Packaging, Transactions of the ASME, **134(**4).

[31] Hao, X., Peng, B., Xie, G., and Chen, Y., 2014, "Thermal Analysis and Experimental Validation of Laminar Heat Transfer and Pressure Drop in Serpentine Channel Heat Sinks for Electronic Cooling," Journal of Electronic Packaging, Transactions of the ASME, **136**(3).

[32] Dai, Z., Fletcher, D. F., and Haynes, B. S., 2015, "Impact of Tortuous Geometry on Laminar Flow Heat Transfer in Microchannels," International Journal of Heat and Mass Transfer, **83**, pp. 382–398.

[33] Al-Neama, A. F., Kapur, N., Summers, J., and Thompson, H. M., 2017, "An Experimental and Numerical Investigation of the Use of Liquid Flow in Serpentine Microchannels for Microelectronics Cooling," Applied Thermal Engineering, **116**, pp. 709–723.

[34] Mousa, M. H., Miljkovic, N., and Nawaz, K., 2021, "Review of Heat Transfer Enhancement Techniques for Single Phase Flows," Renewable and Sustainable Energy Reviews, **137**, p. 110566.

[35] Iga, A., Nishiwaki, S., Izui, K., and Yoshimura, M., 2009, "Topology Optimization for Thermal Conductors Considering Design-Dependent Effects, Including Heat Conduction and Convection," International Journal of Heat and Mass Transfer, **52**(11–12), pp. 2721–2732.

[36] Yoon, G. H., 2010, "Topological Design of Heat Dissipating Structure with Forced Convective Heat Transfer," Journal of Mechanical Science and Technology, **24(**6), pp. 1225–1233.

[37] Alexandersen, J., Aage, N., Andreasen, C. S., and Sigmund, O., 2014, "Topology Optimisation for Natural Convection Problems," International Journal for Numerical Methods in Fluids, **76**(10), pp. 699–721.

[38] Dede, E. M., 2012, "Optimization and Design of a Multipass Branching Microchannel Heat Sink for Electronics Cooling," Journal of Electronic Packaging, Transactions of the ASME, **134**(4).

[39] Koga, A. A., Lopes, E. C. C., Villa Nova, H. F., Lima, C. R. D., and Silva, E. C. N., 2013, "Development of Heat Sink Device by Using Topology Optimization," International Journal of Heat and Mass Transfer, **64**, pp. 759–772.

[40] Yan, S., Wang, F., Hong, J., and Sigmund, O., 2019, "Topology Optimization of Microchannel Heat Sinks Using a Two-Layer Model," International Journal of Heat and Mass Transfer, **143**, p. 118462.

[41] Dong, X., and Liu, X., 2020, "Multi-Objective Optimal Design of Microchannel Cooling Heat Sink Using Topology Optimization Method," Numerical Heat Transfer; Part A: Applications, **77**(1), pp. 90–104.

[42] Li, H., Ding, X., Meng, F., Jing, D., and Xiong, M., 2019, "Optimal Design and Thermal Modelling for Liquid-Cooled Heat Sink Based on Multi-Objective Topology Optimization: An Experimental and Numerical Study," International Journal of Heat and Mass Transfer, **144**, p. 118638.

[43] Lee, J. S., Yoon, S. Y., Kim, B., Lee, H., Ha, M. Y., and Min, J. K., 2021, "A Topology Optimization Based Design of a Liquid-Cooled Heat Sink with Cylindrical Pin Fins Having Varying Pitch," International Journal of Heat and Mass Transfer, **172**, p. 121172.

[44] Laurila, T., Mattila, T., Vuorinen, V., Karppinen, J., Li, J., Sippola, M., and Kivilahti, J. K., 2007, "Evolution of Microstructure and Failure Mechanism of Lead-Free Solder Interconnections in Power Cycling and Thermal Shock Tests," Microelectronics Reliability, **47**(7), pp. 1135–1144.

[45] Subramanian, K. N., 2012, "Reliability of Lead-Free Electronic Solder Interconnects: Roles of Material and Service Parameters," *Lead-Free Solders: Materials Reliability for Electronics*, Wiley Blackwell, pp. 2–9.

[46] Lee, Y. J., Lee, P. S., and Chou, S. K., 2013, "Hotspot Mitigating with Obliquely Finned Microchannel Heat Sink-an Experimental Study," IEEE Transactions on Components, Packaging and Manufacturing Technology, **3**(8), pp. 1332–1341.

[47] Sharma, C. S., Tiwari, M. K., Zimmermann, S., Brunschwiler, T., Schlottig, G., Michel, B., and Poulikakos, D., 2015, "Energy Efficient Hotspot-Targeted Embedded Liquid Cooling of Electronics," Applied Energy, **138**, pp. 414–422.

[48] Sharma, C. S., Schlottig, G., Brunschwiler, T., Tiwari, M. K., Michel, B., and Poulikakos, D., 2015, "A Novel Method of Energy Efficient Hotspot-Targeted Embedded Liquid Cooling for Electronics: An Experimental Study," International Journal of Heat and Mass Transfer, **88**, pp. 684–694.

[49] Frank M. White, 1999, *Fluid Mechanics*, McGraw-Hill International.

[50] Bergman T.L., Levine A.S., Incropera F.P., and Dewitt D.P., 2011, *Fundamentals of Heat and Mass Transfer*, John Wiley & Sons.

[51] Goldberg, D. E., 1994, "Genetic and Evolutionary Algorithms Come of Age," Communications of the ACM, **37**(3), pp. 113–120.

[52] Arora, J. S., Huang, M. W., and Hsieh, C. C., 1994, *Review Papers Methods for Optimization Variables: A Review of Nonlinear Problems with Discrete*, Springer-Verlag.

[53] Hart, P. E., Nilsson, N. J., and Raphael, B., 1968, "A Formal Basis for the Heuristic Determination of Minimum Cost Paths," IEEE Transactions on Systems Science and Cybernetics, **4**(2), pp. 100–107.

[54] Feurtado, M., McPherson, B., Martin, D., McNutt, T., Schupbach, M., Curbow, W. A., Hayes, J., and Sparkman, B., 2019, "High-Performance 300 KW 3-Phase SiC Inverter Based on Next Generation Modular SiC Power Modules," *PCIM Europe 2019; International Exhibition and Conference for Power Electronics, Intelligent Motion, Renewable Energy and Energy Management*.

[55] Feurtado, M., Reeves, M., Martin, D., and McNutt, T., 2020, *Increasing Power Density In Three-Phase Inverters With Direct-Cooled SiC Power Modules*.

[56] Mühlenbein, H., Schomisch, M., and Born, J., 1991, "The Parallel Genetic Algorithm as Function Optimizer," Parallel Computing, **17**(6–7), pp. 619–632.

[57] Kwon, B., Foulkes, T., Yang, T., Miljkovic, N., and King, W. P., 2020, "Air Jet Impingement Cooling of Electronic Devices Using Additively Manufactured Nozzles," IEEE Transactions on Components, Packaging and Manufacturing Technology, **10**(2), pp. 220–229.

[58] Moon, H., Miljkovic, N., and King, W. P., 2020, "High Power Density Thermal Energy Storage Using Additively Manufactured Heat Exchangers and Phase Change Material," International Journal of Heat and Mass Transfer, **153**, p. 119591.

[59] Iradukunda, A. C., Vargas, A., Huitink, D., and Lohan, D., 2020, "Transient Thermal Performance Using Phase Change Material Integrated Topology Optimized Heat Sinks," Applied Thermal Engineering, **179**, p. 115723.

[60] Pilagatti, A. N., Piscopo, G., Atzeni, E., Iuliano, L., and Salmi, A., 2021, "Design of Additive Manufactured Passive Heat Sinks for Electronics," Journal of Manufacturing Processes, **64**, pp. 878–888.

[61] Moon, H., Boyina, K., Miljkovic, N., and King, W. P., 2021, "Heat Transfer Enhancement of Single-Phase Internal Flows Using Shape Optimization and Additively Manufactured Flow Structures," International Journal of Heat and Mass Transfer, **177**, p. 121510.

[62] Ho, J. Y., Liu, P., Leong, K. C., Wong, T. N., and Miljkovic, N., 2021, "A Theoretical Analysis and Parametric Study of Filmwise Condensation on Three-Dimensional Pin Fins," International Journal of Heat and Mass Transfer, **171**, p. 121092.

[63] Agonafer, D., Spector, M. S., and Miljkovic, N., 2021, "Materials and Interface Challenges in High Vapor Quality Two-Phase Flow Boiling Research," IEEE Transactions on Components, Packaging and Manufacturing Technology, pp. 1–1.

[64] Mudawar, I., 2011, "Two-Phase Microchannel Heat Sinks: Theory, Applications, and Limitations," Journal of Electronic Packaging, **133**(4).

[65] Kandlikar, S. G., 2012, "History, Advances, and Challenges in Liquid Flow and Flow Boiling Heat Transfer in Microchannels: A Critical Review," Journal of Heat Transfer, **134**(3).

[66] Upot, N. V., Mahvi, A., Rabbi, K. F., Li, J., Jacobi, A. M., and Miljkovic, N., 2021, "Scalable and Resilient Etched Metallic Micro- and Nanostructured Surfaces for Enhanced Flow Boiling," ACS Applied Nano Materials, **2021**, p. 6658.

[67] Lorenzini, D., and Joshi, Y. K., 2015, "CFD Analysis of Flow Boiling in a Silicon Microchannel With Non-Uniform Heat Flux," ASME 2015 13th International Conference on Nanochannels, Microchannels, and Minichannels, ICNMM 2015, collocated with the ASME 2015 International Technical Conference and Exhibition on Packaging and Integration of Electronic and Photonic Microsystems.

[68] Lorenzini, D., and Joshi, Y., 2019, "Numerical Modeling and Experimental Validation of Two-Phase Microfluidic Cooling in Silicon Devices for Vertical Integration of Microelectronics," International Journal of Heat and Mass Transfer, **138**, pp. 194–207.

[69] Pan, Z., Weibel, J. A., and Garimella, S. v, 2015, "A Cost-Effective Modeling Approach for Simulating Phase Change and Flow Boiling in Microchannels."

[70] Bogojevic, D., Sefiane, K., Walton, A. J., Lin, H., Cummins, G., Kenning, D. B. R., and Karayiannis, T. G., "EXPERIMENTAL INVESTIGATION OF NON-UNIFORM HEATING ON FLOW BOILING INSTABILITIES IN A MICROCHANNELS BASED HEAT SINK."

[71] Lee, J., and Mudawar, I., 2008, "Low-Temperature Two-Phase Micro-Channel Cooling for High-Heat-Flux Thermal Management of Defense Electronics," 2008 11th IEEE Intersociety Conference on Thermal and Thermomechanical Phenomena in Electronic Systems, I-THERM, pp. 132–144.

[72] Konishi, C. A., Qu, W., Jasperson, B., Pfefferkorn, F. E., and Turner, K. T., 2009, "Experimental Study of Adiabatic Water Liquid-Vapor Two-Phase Pressure Drop Across an Array of Staggered Micro-Pin-Fins," ASME International Mechanical Engineering Congress and Exposition, Proceedings, **10**(PART C), pp. 1597–1605.